

Measurements of the $\gamma^*p \rightarrow \Delta$ reaction at low Q^2

N. Sparveris¹, S. Stave², P. Achenbach³, C. Ayerbe Gayoso³, D. Baumann³, J. Bernauer³, A. M. Bernstein², R. Böhm³, D. Bosnar⁶, T. Botto³, A. Christopoulou⁵, D. Dale⁷, M. Ding³, M. O. Distler³, L. Doria³, J. Friedrich³, A. Karabarounis⁵, M. Makek⁶, H. Merkel³, U. Müller³, I. Nakagawa⁴, R. Neuhausen³, L. Nungesser³, C.N. Papanicolas⁵, A. Piegsa³, J. Pochodzalla³, M. Potokar⁸, M. Seimetz³, S. Širca⁸, S. Stiliaris⁵, Th. Walcher³, and M. Weis³

¹ Department of Physics, Temple University, Philadelphia, Pennsylvania 19122

² Department of Physics, Laboratory for Nuclear Science and Bates Linear Accelerator Center, Massachusetts Institute of Technology, Cambridge, Massachusetts 02139, USA

³ Institute für Kernphysik, Johannes Gutenberg-Universität Mainz, D-55099 Mainz, Germany

⁴ Radiation Laboratory, RIKEN, 2-1 Hirosawa, Wako, Saitama 351-0198, Japan

⁵ Institute of Accelerating Systems and Applications and Department of Physics, University of Athens, Athens, Greece

⁶ Department of Physics, University of Zagreb, Croatia

⁷ Department of Physics and Astronomy, University of Kentucky, Lexington, Kentucky 40206 USA

⁸ Institute Jožef Stefan, University of Ljubljana, Ljubljana, Slovenia

Received: date / Revised version: date

Abstract. We report new $p(e, e'p)\pi^0$ measurements in the $\Delta^+(1232)$ resonance at the low momentum transfer region utilizing the magnetic spectrometers of the A1 Collaboration at MAMI. The mesonic cloud dynamics are predicted to be dominant and appreciably changing in this region while the momentum transfer is sufficiently low to be able to test chiral effective calculations. The results disagree with predictions of constituent quark models and are in reasonable agreement with dynamical calculations with pion cloud effects, chiral effective field theory and lattice calculations. The reported measurements suggest that improvement is required to the theoretical calculations and provide valuable input that will allow their refinements.

PACS. 13.60.Le Meson production – 13.40.Gp Electromagnetic form factors

1 Introduction

Hadrons are composite systems with complex quark-gluon and meson cloud dynamics that give rise to non-spherical components in their wavefunction which in a classical limit and at large wavelengths will correspond to a "deformation". In recent years an extensive experimental and theoretical effort has been focused on identifying and understanding the origin of possible non-spherical amplitudes in the nucleon wavefunction [1, 2, 3, 4, 5, 6, 7, 8, 9, 10, 11, 12, 13, 14, 15, 16, 17, 18, 19, 20, 21, 22, 23, 24, 25, 26, 27, 28, 29, 30]. The spectroscopic quadrupole moment provides the most reliable and interpretable measurement of such amplitudes. For the proton, the only stable hadron, it vanishes identically because of its spin 1/2 nature. Instead, the signature of the non-spherical components of the proton is sought in the presence of resonant quadrupole amplitudes ($E_{1+}^{3/2}$, $S_{1+}^{3/2}$) in the predominantly magnetic dipole ($M_{1+}^{3/2}$) $\gamma^*N \rightarrow \Delta$ transition. Nonvanishing resonant quadrupole amplitudes will signify that either the proton or the $\Delta^+(1232)$ or more likely both are characterized by non-spherical components in their wavefunctions.

In the constituent-quark picture of hadrons, the non-spherical amplitudes are a consequence of the non-central, color-hyperfine interaction among quarks [31]. However, it has been shown that this mechanism only provides a small fraction of the observed quadrupole signal at low momentum transfers, with the magnitudes of this effect for the predicted E2 and C2 amplitudes [32] being at least an order of magnitude too small to explain the experimental results and with the dominant M1 matrix element being $\simeq 30\%$ low. A likely cause of these dynamical shortcomings is that the quark model does not respect chiral symmetry, whose spontaneous breaking leads to strong emission of virtual pions (Nambu-Goldstone Bosons)[33]. These couple to nucleons as $\sigma \cdot \mathbf{p}$ where σ is the nucleon spin, and \mathbf{p} is the pion momentum. The coupling is strong in the p wave and mixes in non-zero angular momentum components. Based on this, it is physically reasonable to expect that the pionic contributions increase the M1 and dominate the E2 and C2 transition matrix elements in the low Q^2 (large distance) domain. This was first indicated by adding pionic effects to quark models[34, 35, 36], subsequently in

pion cloud model calculations [20, 21], and recently demonstrated in effective field theory (chiral) calculations [37].

An experimental effort of many years, where MAMI and Bates/MIT have focused at the low and medium momentum transfer region while JLab has offered measurements up to $Q^2 = 7.7$ (GeV/c)², has allowed the extensive exploration of the resonant quadrupole amplitudes [3, 4, 5, 6, 7, 8, 9, 10, 11, 12, 13, 14, 15, 16, 17, 18, 26, 27, 28, 29, 30]. The experimental results (the ratios $CMR = Re(S_{1+}^{3/2}/M_{1+}^{3/2})$ and $EMR = Re(E_{1+}^{3/2}/M_{1+}^{3/2})$ are routinely used to present the relative magnitude of the amplitudes of interest) are in reasonable agreement with models invoking the presence of nonspherical components in the nucleon wavefunction. With the existence of these amplitudes well established, recent investigations have focused on testing the reaction calculations and reducing the experimental errors and the theoretical uncertainties in extracting the rather small resonant multipoles from the data. In order to fully exploit the experimental capabilities one has to explore all three reaction channels associated with the $\gamma^*N \rightarrow \Delta$ transition: $H(e, e'p)\pi^0$, $H(e, e'p^+)n$ and $H(e, e'p)\gamma$. Furthermore, it is also important to control the effect of the background contributions which play a more significant role off resonance and that are also dominant in the TL' (fifth structure function) observable. Extending the momentum transfer range of the measurements, providing measurements of higher precision, exploring further the wings of the resonance which provides valuable sensitivity to the background amplitude contributions and measurement of the practically unexplored photon excitation channel can contribute toward a more accurate description of the nucleon resonance and can offer a better understanding of the underlying nucleon dynamics. In this paper a high precision measurement of the CMR at $Q^2 = 0.127$ (GeV/c)² is presented in the region where the pion cloud plays a significant role. Furthermore, measurements at $Q^2 = 0.20$ (GeV/c)² demonstrate that the dynamical models are not accurately calculating the background amplitudes which are needed to describe the data away from the resonance energy.

2 The Experiment

In this work we have explored the low momentum transfer region with new measurements of the π^0 reaction channel that are particularly sensitive to the meson cloud dynamics. New measurements have been performed at $Q^2 = 0.127$ (GeV/c)². These measurements offer the extraction of the Coulomb quadrupole amplitude with a better precision than the previous MAMI measurement [6] and allow an important cross check to the corresponding (same momentum transfer) measurements performed in other labs [12, 13]. Furthermore, the data set at $Q^2 = 0.20$ (GeV/c)² from [27] has been further analyzed by fully exploiting the previously unexplored wide phase space coverage of these measurements to study the dependence of the amplitudes on the center-of-mass energy W ; this analysis was motivated by the strong deviations of the theoretical model

predictions as a function of the center-of-mass energy in the measured region. The differential partial cross sections of the reaction have been extracted at $Q^2 = 0.20$ (GeV/c)² as a function of the center-of-mass energy W with high precision and offer strong experimental constraints that allow to resolve these theoretical discrepancies.

The cross section of the $p(e, e'p)\pi^0$ reaction is sensitive to five independent partial responses ($\sigma_T, \sigma_L, \sigma_{LT}, \sigma_{TT}$ and $\sigma_{LT'}$) [24] :

$$\frac{d^5\sigma}{d\omega d\Omega_e d\Omega_{pq}^{cm}} = \Gamma(\sigma_T + \epsilon\sigma_L - v_{LT}\sigma_{LT} \cos\phi_{pq}^* + \epsilon\sigma_{TT} \cos 2\phi_{pq}^* - h\cdot p_e \cdot v_{LT'}\sigma_{LT'} \sin\phi_{pq}^*)$$

where $v_{LT} = \sqrt{2\epsilon(1+\epsilon)}$ and $v_{LT'} = \sqrt{2\epsilon(1-\epsilon)}$ are kinematic factors, ϵ is the transverse polarization of the virtual photon, Γ the virtual photon flux, $h = \pm 1$ is the electron helicity, p_e is the magnitude of the electron longitudinal polarization, and ϕ_{pq}^* is the proton azimuthal angle with respect to the electron scattering plane. The differential cross sections ($\sigma_T, \sigma_L, \sigma_{LT}, \sigma_{TT}$ and $\sigma_{LT'}$) are all functions of the center of mass energy W , the four momentum transfer squared Q^2 , and the proton center of mass polar angle θ_{pq}^* (measured from the momentum transfer direction) [24].

The $\sigma_0 = \sigma_T + \epsilon\sigma_L$ response is dominated by the M_{1+} resonant multipole. The interference of the $C2$ and $E2$ amplitudes with the $M1$ dominates the Longitudinal - Transverse (LT) and Transverse - Transverse (TT) responses respectively. The $\sigma_{LT'}$ response [24] provides sensitivity to background contributions [40] primarily through the $Im(S_{0+}^*M_{1+})$ term; as a result the real part of S_{0+} is manifested through interference with the dominant imaginary part of M_{1+} .

The experiment was performed at the Mainz Microtron using the A1 magnetic spectrometers [41] in an arrangement reported in [28, 42]. An 855 MeV polarized electron beam was employed on a liquid-hydrogen target. The beam energy has an absolute uncertainty of ± 160 keV and a spread of 30 keV (FWHM). Beam polarization was measured periodically with a Møller polarimeter to be $\approx 75\%$. The beam average current was 25 μA . Electrons and protons were detected in coincidence with spectrometers A and B respectively. Both spectrometers use two pairs of vertical drift chambers respectively for track reconstruction and two layers of scintillator detectors for timing information and particle identification [41]. Spectrometer B allows out-of-plane detection capability of up to 10° with respect to the horizontal plane which in the center of mass frame corresponds to much larger values. Out of plane angles, ϕ_{pq}^* , up to 90° were accessed in our measurements thus allowing the isolation of the fifth response. Measurements with the proton spectrometer at three different azimuthal angles, ϕ_{pq}^* , for the same central kinematics in W, Q^2 and θ_{pq}^* allowed the extraction of all three unpolarized partial cross sections σ_{TT}, σ_{LT} and $\sigma_0 = \sigma_T + \epsilon\sigma_L$.

Measurements were performed at $Q^2 = 0.20$ (GeV/c)² for proton angles of $\theta_{pq}^* = 34^\circ$ and 57° , covering a center-of-mass energy range from $W = 1205$ MeV to 1240 MeV .

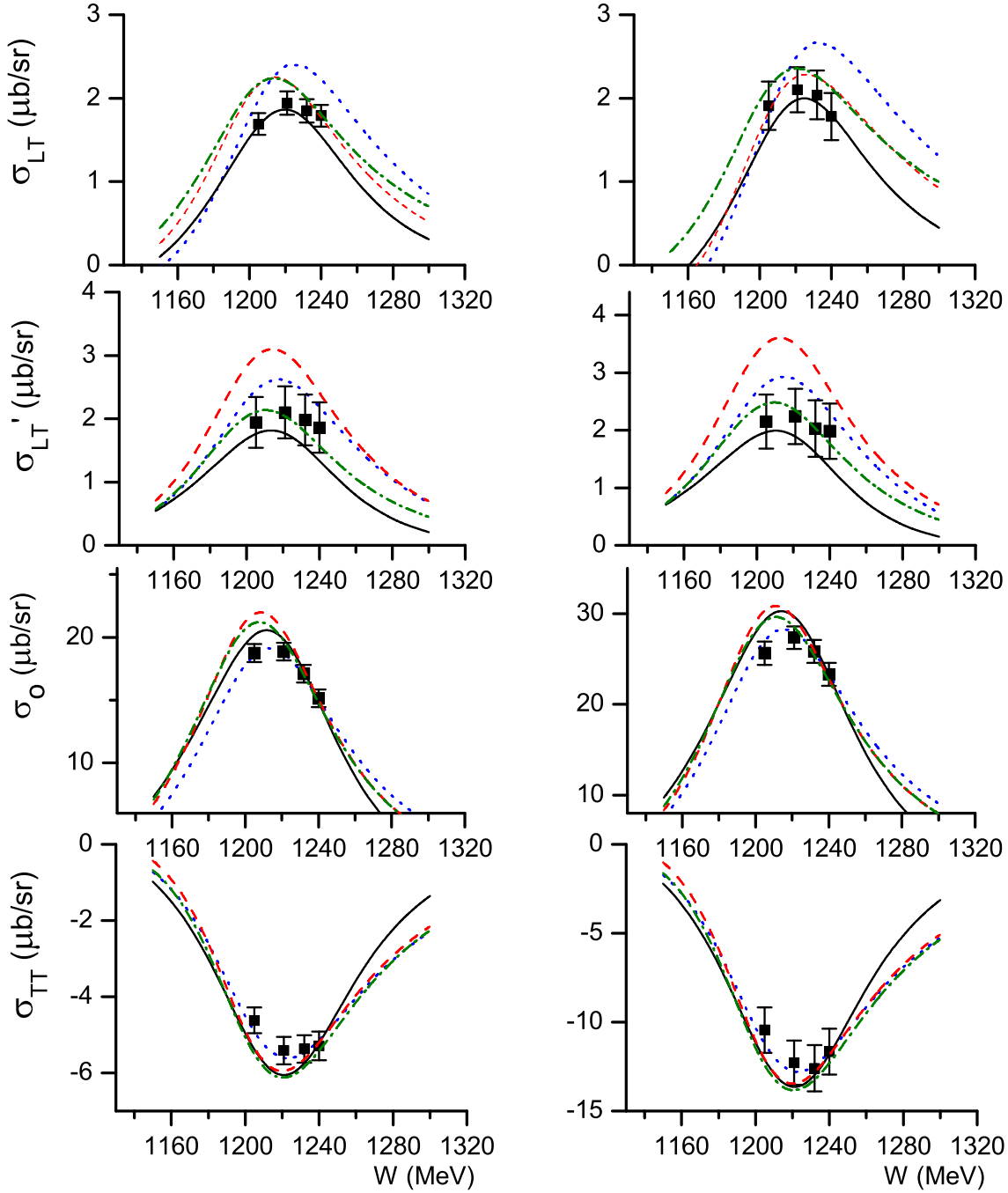


Fig. 1. Extracted values for σ_{LT} , $\sigma_{LT'}$, σ_0 and σ_{TT} (from top to bottom) at $Q^2 = 0.20$ (GeV/c)². Left panels correspond to $\theta_{pq}^* = 34^\circ$ while the right panels to $\theta_{pq}^* = 57^\circ$. The theoretical predictions of DMT (dot), SAID (dash-dot), MAID (dash) and Sato Lee (solid) are also presented.

At each θ_{pq}^* kinematics the proton spectrometer was sequentially placed at three different azimuthal ϕ_{pq}^* angles (0° , 90° , 180° and 38° , 142° , 180° respectively) which allowed to isolate the σ_{TT} , σ_{LT} and $\sigma_0 = \sigma_T + \epsilon \cdot \sigma_L$ partial cross sections. The cross sections were obtained from the parts of the phase space which were matched in (W, Q^2, θ_{pq}^*) for all three ϕ_{pq}^* measurements. Furthermore,

the out of plane measurements allowed the extraction of the $\sigma_{LT'}$ cross section. The partial cross sections were extracted for center-of-mass energies $W = 1205, 1221, 1232$ and 1240 MeV. A second set of three sequential ϕ_{pq}^* measurements (0° , 90° , 180°) at $Q^2 = 0.127$ (GeV/c)² and $\theta_{pq}^* = 28^\circ$ allowed the extraction of the partial cross sections at $W = 1232$ MeV. Point cross sections were derived

from the finite acceptances by projecting the measured values using theoretical models [20, 21, 22, 23, 24, 25] while the projection to central values had a minimal influence on the systematic error. SIMUL++ [43] is the simulation software that was employed to calculate the multidimensional kinematical phase space. Acceptance cuts were utilized in order to limit the analysis to the central region of the spectrometers and to ensure that any possible edge effects will be avoided. Radiative corrections were applied to the data using the Monte Carlo simulation; a detailed description of these corrections can be found in [42]. Systematic uncertainties were reduced by using Spectrometer C throughout the experiment as a luminosity monitor. Elastic scattering data from H and ^{12}C for calibration purposes were taken at 600 MeV. The systematic uncertainty of the cross sections [42] is at the level of 3% to 4%. The main contributions to the systematic uncertainty came from uncertainties to the luminosity, phase space, angular and momentum resolution of the spectrometers, beam position and the model uncertainty for the extraction of point cross sections. The luminosity uncertainty comes from a 1% uncertainty in the target length and a 1% uncertainty in the density (these uncertainties have been conservatively added linearly). The phase-space cut uncertainties corresponding to the stability of the results to the variation of the size of the kinematic phase space cuts are typically to the order of 1.5%. The spectrometer angular and momentum resolution resulted to an uncertainty of 1%. The spectrometer positioning uncertainties of 0.6 mm and 0.1 mrad are much smaller than the resolution uncertainties and thus do not affect significantly the results. The beam position had a systematic effect of 1% to the cross section while the model uncertainty for the extraction of point cross sections was typically at the 0.5% level. Systematics were the dominant uncertainty factor in this experiment since the statistical uncertainties are typically smaller than 1%.

3 Results and Discussion

The experimental results are presented in Table 1 and Table 2 while the measured partial cross sections are plotted in figs. 1 and 2. Figure 1 shows σ_{LT} , $\sigma_{LT'}$, σ_{TT} and σ_0 as a function of the center-of-mass energy at $Q^2 = 0.20 \text{ (GeV/c)}^2$. The new measurements come to complete the exploration performed at the same momentum transfer [27] and cover a center-of-mass energy range where the theoretical calculations exhibit significant disagreement to their predictions. The precision of the new measurements allows to resolve these model discrepancies. The experimental results are compared with the SAID multipole analysis [25], the phenomenological model MAID 2007 [23, 22] and the dynamical model calculations of Sato-Lee [20] and of DMT (Dubna - Mainz - Taipei) [21]. The Sato-Lee (SL) [20] and DMT [21] are dynamical reaction models which include pionic cloud effects. Both calculate the resonant channels from dynamical equations. DMT uses the background amplitudes of MAID with some small modifications. Sato-Lee calculate all amplitudes consistently

Table 1. Extracted values for $\sigma_0, \sigma_{LT}, \sigma_{TT}$ and $\sigma_{LT'}$ at $Q^2 = 0.20 \text{ (GeV/c)}^2$. The uncertainties correspond to the statistical and the systematic uncertainties, respectively.

W (MeV)	θ_{pq}^* ($^\circ$)	σ	$\sigma \text{ (}\mu\text{b/sr)}$
1205	34	σ_0	$18.75 \pm 0.21 \pm 0.69$
1205	34	σ_{LT}	$1.69 \pm 0.05 \pm 0.13$
1205	34	σ_{TT}	$-4.62 \pm 0.15 \pm 0.30$
1205	34	$\sigma_{LT'}$	$1.94 \pm 0.21 \pm 0.34$
1221	34	σ_0	$18.86 \pm 0.21 \pm 0.68$
1221	34	σ_{LT}	$1.94 \pm 0.06 \pm 0.12$
1221	34	σ_{TT}	$-5.41 \pm 0.16 \pm 0.32$
1221	34	$\sigma_{LT'}$	$2.10 \pm 0.22 \pm 0.35$
1232	34	σ_0	$17.10 \pm 0.20 \pm 0.68$
1232	34	σ_{LT}	$1.85 \pm 0.06 \pm 0.13$
1232	34	σ_{TT}	$-5.37 \pm 0.16 \pm 0.33$
1232	34	$\sigma_{LT'}$	$1.98 \pm 0.21 \pm 0.34$
1240	34	σ_0	$15.14 \pm 0.19 \pm 0.67$
1240	34	σ_{LT}	$1.79 \pm 0.06 \pm 0.12$
1240	34	σ_{TT}	$-5.29 \pm 0.16 \pm 0.32$
1240	34	$\sigma_{LT'}$	$1.86 \pm 0.20 \pm 0.35$
1205	57	σ_0	$25.64 \pm 0.47 \pm 1.20$
1205	57	σ_{LT}	$1.91 \pm 0.11 \pm 0.27$
1205	57	σ_{TT}	$-10.44 \pm 0.60 \pm 1.13$
1205	57	$\sigma_{LT'}$	$2.15 \pm 0.25 \pm 0.40$
1221	57	σ_0	$27.36 \pm 0.49 \pm 1.14$
1221	57	σ_{LT}	$2.10 \pm 0.12 \pm 0.24$
1221	57	σ_{TT}	$-12.28 \pm 0.66 \pm 1.06$
1221	57	$\sigma_{LT'}$	$2.24 \pm 0.26 \pm 0.41$
1232	57	σ_0	$25.82 \pm 0.47 \pm 1.18$
1232	57	σ_{LT}	$2.04 \pm 0.12 \pm 0.26$
1232	57	σ_{TT}	$-12.60 \pm 0.66 \pm 1.12$
1232	57	$\sigma_{LT'}$	$2.03 \pm 0.25 \pm 0.42$
1240	57	σ_0	$23.29 \pm 0.46 \pm 1.18$
1240	57	σ_{LT}	$1.78 \pm 0.10 \pm 0.26$
1240	57	σ_{TT}	$-11.66 \pm 0.63 \pm 1.12$
1240	57	$\sigma_{LT'}$	$1.98 \pm 0.24 \pm 0.41$

Table 2. Extracted values for σ_0, σ_{LT} and σ_{TT} at $Q^2 = 0.127 \text{ (GeV/c)}^2$. The uncertainties correspond to the statistical and the systematic uncertainties, respectively.

W (MeV)	θ_{pq}^* ($^\circ$)	σ	$\sigma \text{ (}\mu\text{b/sr)}$
1232	28	σ_0	$15.51 \pm 0.20 \pm 0.65$
1232	28	σ_{LT}	$1.62 \pm 0.13 \pm 0.16$
1232	28	σ_{TT}	$-3.98 \pm 0.16 \pm 0.32$

within the same framework with only three free parameters. Both find that a large fraction of the quadrupole multipole strength arises due to the pionic cloud with the effect reaching a maximum value in this momentum transfer region. Sato-Lee offers a good description of the data slightly overestimating σ_0 at the lower wing of the resonance. DMT is in good agreement with all partial cross sections except σ_{LT} indicating that the Coulomb quadrupole amplitude is significantly overestimated. The SAID multipole analysis [25] and the MAID model [22, 23] which offers a flexible phenomenology may agree with

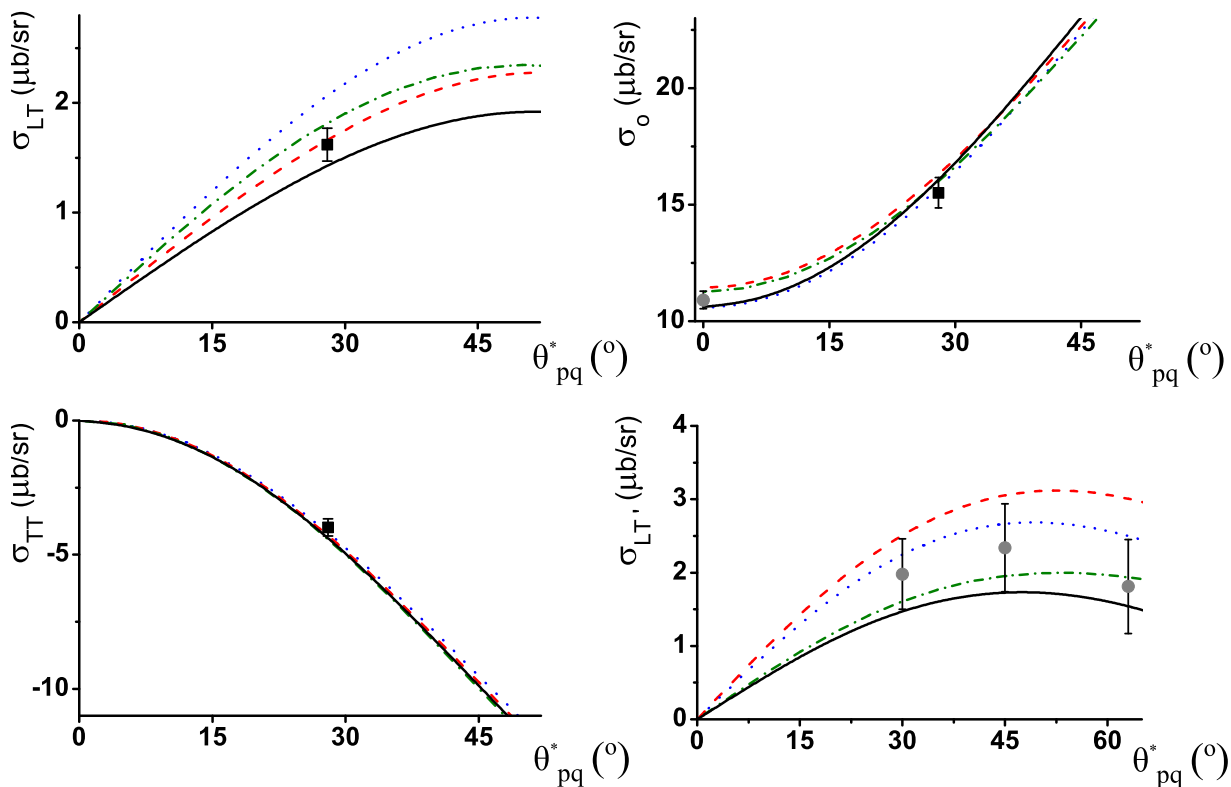


Fig. 2. Extracted values for σ_{LT} , $\sigma_{LT'}$, σ_0 and σ_{TT} at $Q^2 = 0.127$ (GeV/c)² and $W=1232$ MeV (square symbols). The MAMI measurements from [28] are also shown (circle symbols). The theoretical predictions of DMT (dot), SAID (dash-dot), MAID (dash) and Sato Lee (solid) are also presented.

all measurements at $W=1232$ MeV but they tend to systematically overestimate all partial cross sections at the lower wing of the resonance. Furthermore MAID exhibits a significant overestimation of the fifth structure function $\sigma_{LT'}$ thus indicating that a re-adjustment is needed both in the resonant and in the background amplitudes. Figure 2 shows the partial cross section measurements as a function of θ_{pq}^* at $Q^2 = 0.127$ (GeV/c)². The comparison of the measurements with the theoretical calculations is consistent with the data-model comparison at $Q^2 = 0.20$ (GeV/c)². DMT is overestimating the σ_{LT} (and the Coulomb quadrupole amplitude) while MAID tends to overestimate the fifth structure function. All other observables are in good agreement with the theoretical predictions. Nevertheless this does not guarantee the success of any of the models; the $Q^2 = 0.20$ (GeV/c)² measurements are also in good agreement with the theoretical calculations at the same center-of-mass energy but at the same time they exhibit a strong disagreement at the lower wing of the resonance.

Fits of the resonant amplitudes have been performed at $Q^2 = 0.127$ (GeV/c)² while taking into account the contributions of background amplitudes from MAID, DMT, SAID and Sato Lee models. The fitting procedure used in this analysis is described in detail in [28,42]. The models differ in their description of the background terms thus

leading to a deviation of the fitted results which indicates the level of the model uncertainty. We adopt the RMS deviation of the fitted central values as the model uncertainty of the extracted amplitudes. Fits were also performed where background amplitudes, such as S_{0+} , were allowed to vary in addition to the resonant amplitudes. They resulted in successful descriptions of $\sigma_{LT'}$ but the difference in the derived resonant amplitude results from those of the resonant-only parameter fits were inconsequential. The resonant value for the CMR is $(-5.25 \pm 0.61_{stat+sys} \pm 0.30_{model})\%$. A measurement of the $M_{1+}^{3/2} = (39.99 \pm 1.04_{stat+sys} \pm 0.60_{model})(10^{-3}/m_{\pi^+})$ is also provided through this experiment. The extracted value for the Coulomb quadrupole amplitude is found in agreement with previous measurements [6, 12, 13]. For the Bates/MIT measurements the CMR extraction is driven by the σ_{LT} measurements of [12], which when compared to the cross section measurements of this work tend to be systematically higher (but in agreement within the experimental uncertainties), thus leading to a higher CMR ratio for Bates/MIT but within experimental agreement to this MAMI measurement.

The derived CMR value indicates a rather smooth momentum transfer variation toward the lowest Q^2 data point (see fig. 3). No evidence of any local dip inside the Q^2

0.06 – 0.20 $(GeV/c)^2$ region is supported by this measurement, while this result is found to be in good agreement with the measurements of [6, 13]. The SAID, MAID, DMT and Sato Lee models are in qualitative agreement with the experimental results but detailed improvements could and should be implemented to all of these calculations; the measurements presented in this work provide strong experimental constraints and offer valuable information in order to improve the weaknesses of the theoretical calculations. Constituent quark model (CQM) predictions are known to considerably deviate from the experimental results, grossly underestimating the resonant amplitudes. Two representative CQM calculations are shown in fig. 3, that of Capstick [2] and of the hypercentral quark model (HQM) [39], which fail to describe the data. It demonstrates that the color hyperfine interaction is inadequate to explain the effect at least at large distances. Effective field theoretical (chiral) calculations [37, 38], that are solidly based on QCD, successfully account for the magnitude of the effects giving further credence to the dominance of the meson cloud effect. Results from lattice QCD [19] are accurate enough to allow a comparison to experiment with the chirally extrapolated [37] values of CMR found to be nonzero and negative in the low Q^2 region. Obtaining lattice results of higher precision using lighter quark masses and further refining the chiral extrapolation procedure will offer a more meaningful comparison in the near future.

4 Conclusion

Cross section measurements for π^0 electroproduction in the $\Delta(1232)$ resonance have been performed at the low momentum transfer region where the mesonic cloud dynamics are predicted to be dominant and appreciably changing and a precision measurement of the Coulomb quadrupole amplitude has been achieved. The partial cross sections have been measured as a function of the proton center of mass polar angle and of the center of mass energy in a kinematic range where the predictions of the theoretical calculations exhibit significant differences. The strong experimental constraints provided by the new results offer valuable input in order to improve the model discrepancies. The measured resonant amplitudes are in disagreement with the values predicted by quark models on account of the noncentral color-hyperfine interaction. The momentum transfer region is sufficiently low to be able to test chiral effective calculations. The results are in qualitative agreement with lattice calculations, with chiral perturbation theory calculations and with dynamical models which explicitly include the pion cloud. Nevertheless all of these calculations require further refinements in order to obtain quantitative agreement with experiment. For the dynamical models the experimental data demonstrate that the background amplitudes, which are needed to describe the data away from the resonance energy, are not accurately calculated.

We would like to thank the MAMI accelerator group and the MAMI polarized beam group for the excellent

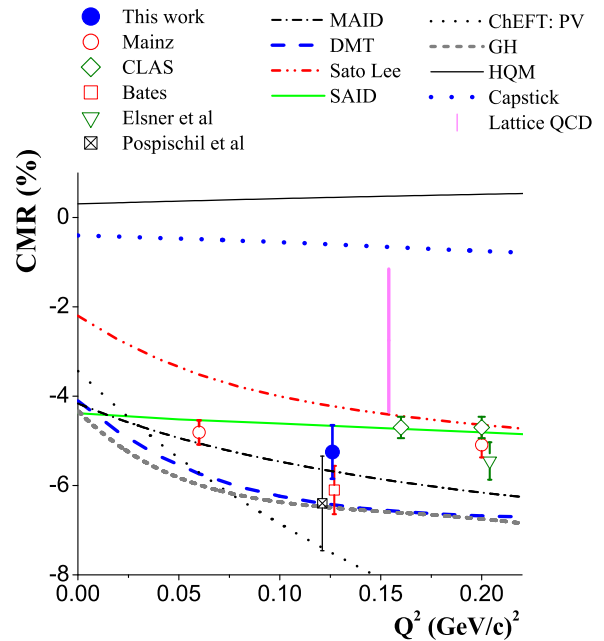


Fig. 3. Measurements for CMR (errors include statistical and systematic uncertainties) as a function of Q^2 . The result from this work (solid circle) and the experimental results from [6, 13, 15, 26, 27, 29] (open symbols) are presented. The theoretical predictions of MAID, DMT, SAID, Sato-Lee, Capstick, HQM, the Lattice-QCD calculation, ChEFT of Pascalutsa-Vanderhaegen and the Gail-Hemmert are also shown.

beam quality combined with a continuous high polarization. This work is supported by the National Science Foundation.

References

1. A. de Rujula, H. Georgi and S.L. Glashow *et al.*, *Phys. Rev. D* **12**, 147 (1975).
2. N. Isgur, G. Karl and R. Koniuk, *Phys. Rev.* **D25**, 2394 (1982).
3. G. Blanpied *et al.*, *Phys. Rev. Lett.* **79**, 4337 (1997).
4. R. Beck *et al.*, *Phys. Rev. Lett.* **78**, 606 (1997); *ibid.* **79**, 4515 (1997) (Erratum).
R. Beck *et al.*, *Phys. Rev.* **C61**, 35204 (2000).
5. V.V. Frolov *et al.*, *Phys. Rev. Lett.* **82**, 45 (1999).
6. T. Pospischil *et al.*, *Phys. Rev. Lett.* **86**, 2959 (2001).
7. C. Mertz *et al.*, *Phys. Rev. Lett.* **86**, 2963 (2001).
8. P. Bartsch *et al.*, *Phys. Rev. Lett.* **88**, 142001 (2002).
9. L.D. van Buuren *et al.*, *Phys. Rev. Lett.* **89**, 12001 (2002).
10. K. Joo *et al.*, *Phys. Rev. Lett.* **88**, 122001 (2002).
11. N.F. Sparveris *et al.*, *Phys. Rev.* **C67**, 058201 (2003).
12. C. Kunz *et al.*, *Phys. Lett.* **B 564**, 21 (2003).
13. N.F. Sparveris *et al.*, *Phys. Rev. Lett.* **94**, 022003 (2005).
14. J.J. Kelly *et al.*, *Phys. Rev. Lett.* **95**, 102001 (2005).
15. S. Stave *et al.*, *Eur. Phys. J.* **A 30**, 471 (2006).
16. K. Joo *et al.*, *Phys. Rev.* **C68**, 032201 (2003).
17. K. Joo *et al.*, *Phys. Rev.* **C70**, 042201 (2004).
18. M. Ungaro *et al.*, *Phys. Rev. Lett.* **97**, 112003 (2006).

19. C. Alexandrou *et al.*, Phys. Rev. Lett. **94**, 021601 (2005); Phys. Rev. **D77** 085012 (2008); Phys. Rev. **D83** 014501 (2011).
20. T. Sato and T.-S.H. Lee, Phys. Rev. **C63**, 055201 (2001).
21. S.S. Kamalov and S. Yang, Phys. Rev. Lett. **83**, 4494 (1999)
22. S.S. Kamalov *et al.*, Phys. Lett. **B 522**, 27 (2001).
23. D. Drechsel *et al.*, Nucl. Phys. **A 645**, 145 (1999).
24. D. Drechsel and L. Tiator, J. Phys. **G18**, 449 (1992)
25. R.A. Arndt, *et al.* Phys. Rev. **C66**, 055213 (2002); nucl-th/0301068 and <http://gwdac.phys.gwu.edu>
26. D. Elsner *et al.*, Eur. Phys. J. **A 27** 91-97 (2006).
27. N. F. Sparveris *et al.*, Phys. Lett. **B651**, 102 (2007).
28. S. Stave *et al.*, Phys. Rev. **C78**, 025209 (2008)
29. I. G. Aznauryan *et al.*, Phys. Rev. **C80**, 055203 (2009)
30. A. N. Villano *et al.*, Phys. Rev. **C80**, 035203 (2009)
31. S.L. Glashow, Physica 96A, 27 (1979); N. Isgur, G. Karl and R. Koniuk, Phys. Rev. **D25**, 2394 (1982).
32. S. Capstick and G. Karl, Phys. Rev. **D41**, 2767 (1990).
33. A.M. Bernstein, Eur. Phys. J. **A 17**, 349 (2003).
34. D.-H. Lu, A. W. Thomas, and A. G. Williams, Phys. Rev. **C55**, 3108 (1997).
35. U. Meyer, E. Hernandez, and A. J. Buchmann, Phys. Rev. **C64**, 035203 (2001).
36. M. Fiolhais, B. Golli, and S. Sirca, Phys. Lett. **B373**, 229 (1996).
37. V. Pascalutsa and M. Vanderhaegen *et al.*, Phys. Rev. **D73**, 034003 (2006).
38. T. A. Gail and T. R. Hemmert, Eur. Phys. J. **A 28** (1), 91-105 (2006).
39. M. De Sanctis *et al.*, Nucl. Phys. **A 755**, 294 (2005).
40. W. Mandeville *et al.*, Phys. Rev. Lett. **72**, 3325-3328 (1994).
41. K.I. Blomqvist *et al.*, Nucl. Instrum. Methods **A 403**, 263 (1998).
42. S. Stave, Ph.D. thesis, MIT, 2006.
43. M. O. Distler, H. Merkel, and M. Weis, in Proceedings of the 12th IEEE Real Time Congress on Nuclear and Plasma Sciences, Valencia, Spain, 2001, edited by E. Sanchis Peris, A. Ferrer Soria, and V. Gonzalez Millan (IEEE, New York, 2001).